Weiwei LIU, Hongfa DING[1], Xianzhong DUAN[1], Liang LI[1], Fritz HERLACH[2]

Huazhong University of Science and Technology (1), Katholieke Universiteit, Leuven (2)

A Novel Control Strategy for the Power Supply to Achieve the 45 T / 600 ms Flat-Top Field

Abstract. *In order to achieve the 45* T */ 600* ms *flat-top field, one type of high-field quasi-continuous magnets (HFQCM) and a power supply system related are now under construction at the Wuhan National High Magnetic Field Center (WHMFC). Considering the temperature rise of the magnet and ripple minimization, the topology and the novel repetitive control method of the power supply system is detailed. Simulated results are provided to validate the proposed method.*

Streszczenie. *Aby wytworzyć pole magnetyczne 45 T/600 ms opracowano specjalny typ układu zasilającego. Uwzględniono ryzyko wzrostu temperatury i potrzebę minimalizacji zafalowań. (**Nowa metod sterowania układem zasilania elektromagnesu umożliwiająca otrzymanie pola magnetycznego 45 T**)*

Keywords: high-field quasi-continuous magnets, phase-controlled rectifier, dc passive filter, repetitive control.
Słowa kluczowe: pole magnetyczne, układ zasilania, elektromagnes.

Introduction

A wide variety of high-field magnet systems will be developed and operated at the Wuhan National High Magnetic Field Center (WHMFC) at Wuhan, China, with support from the National Development and Reformation Committee. Basic scientific research such as biology, chemistry, geology, material science engineering, medicine and solid-state physics, can then be carried out in this extreme physical environment. Research under high magnetic field conditions sometimes requires the magnetic field to be as constant as possible [1, 2, 3]. To meet the low -ripple requirement, one nitrogen-cooled, 45 T / 600 ms high-field quasi-continuous magnet (HFQCM) was specified to obtain the best performance available at the required high power level to be provided by industrial power supplies.

In order to energize the HFQCM, a hybrid power supply, consisting of a 12-pulse phase-controlled rectifier (PCR) in parallel with a dc passive filter (DCPF), is proposed. The pulsed power and energy for the PCR is provided by a 100 MVA / 100 MJ flywheel pulse generator (FPG), which has been installed and commissioned at the WHMFC [4]. Two three-winding step-down 6.9 kV / 0.66 kV transformers, connecting the FPG and the PCR, are now under construction. The dc ripple during the flat-top period is reduced by the DCPF. With this scheme, the large power handling capability of the PCR and the good filtering ability of the DCPF are fully utilized in a complementary way.

A novel control method that implements the desired magnetic field waveform for the PCR is proposed. Due to the high current flowing through the magnet, the temperature rises due to the increase of the resistance, which may have a negative influence on the control of the magnetic field waveform. Using the current reference profile, the magnet resistance model is utilized to predict the required output voltage waveform.

The operating principles of the power circuit and the control scheme are discussed in the paper. A design example is given and simulated results are provided to validate the proposed structure and control scheme.

Power supply configuration

The design of the power supply system for the 45 T / 600 ms magnet is mainly driven by the constraints governing the magnet design and only to a lesser degree by limitations of power supply components and schemes, and limitations given by the power source [5 ,6, 7]. The identical modules use a thyristorized preregulator, which is a 12-pulse PCR. Fig. 1 shows the schematic of the proposed power supply module.

In this hybrid structure, the FPG (Part 1) has been assembled and installed already at the WHMFC. The PCR (Part 2) is now under construction, while the DCPF (Part 3) is under design. The PCR is designed to handle the bulk of the output power, whereas the DCPF is only used for harmonic cancellation under transient conditions.

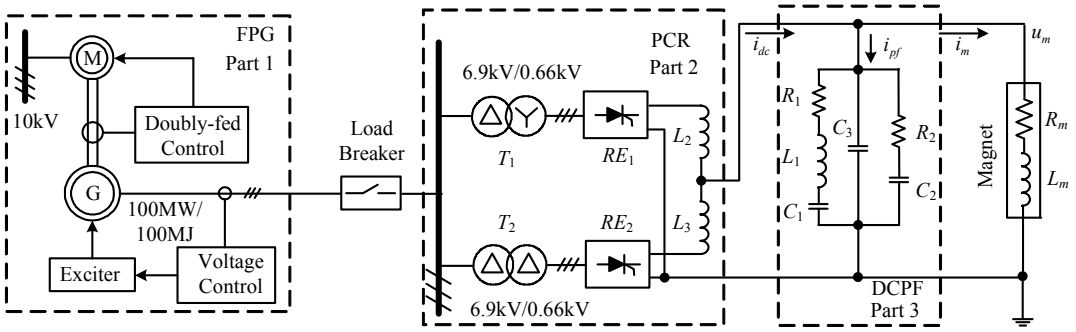

Fig. 1 Circuit diagram of the power supply system.

2.1 FPG

The FPG system is composed of an induction motor and a synchronous generator [8]. A doubly fed control system is utilized to raise the rotating speed of the FPG to the original maximum speed 713 rpm. At this speed, the maximum rotating speed of the generator, about 185 MJ are stored in the shaft train. The upper speed limit for pulse operation is 713 rpm (95 Hz) and the lower limit is 495 rpm (66 Hz),

allowing up to about 100 MJ to be extracted with a duration of 4 seconds every 2 minutes. In the present configuration of the FPG system, pulses are usually started at 594 rpm to limit fatigue of the rotor materials. The exciter and the voltage control system collaborate to stabilize the generator output voltage to be constant over the energizing period of the pulse.

2.2 PCR

Two independent 6-pulse rectifiers, connected in parallel through a smoothing reactor, resulting in a 12-pulse PCR, are identical and are fed from the FPG. The power of the 12-pulse PCR is provided by two 9.66 MVA transformer stations, whose primary windings are connected to the 6.9 kV transmission system, while the secondary voltages are 0.66 kV. A ±10% tap changer allows slow voltage adjustments to satisfy varied needs of magnets. One of the transformers is a Δ-Δ unit and the other a Δ-Y unit, producing the two 30º phase shifted three phase systems needed for the 12-pulse PCR prototype. One set of underground cables, which connects the FPG to the WHFMC laboratory, is connected to a load breaker.

2.3 DCPF

The PCR will produce even-numbered ripple (1.14 kHz to 0.79 kHz mainly) of the ac system frequency in the dc circuit. For the HFQCM, the ripple should be filtered out. One DCPF is connected at the output of the PCR. It consists of a single tuned filter branch, a capacitor branch and an R-C damping branch. At the output of the FPG, the voltage waveform can be smoothed [9, 10]. The DCPF structure in reference [10] is utilized to build the filtering system. The DCPF parameters are given in the Appendix.

The transfer function for the DCPF of Fig. 1 can be calculated as follows,

$$Z_{pf} = 1/\left[(1/Z_1)+(1/Z_2)+(1/Z_3)\right] \tag{1}$$

where

$$\begin{cases} Z_1 = R_1 + sL_1 + (1/sC_1) \\ Z_2 = R_2 + (1/sC_2) \\ Z_3 = (1/sC_3) \end{cases} \tag{2}$$

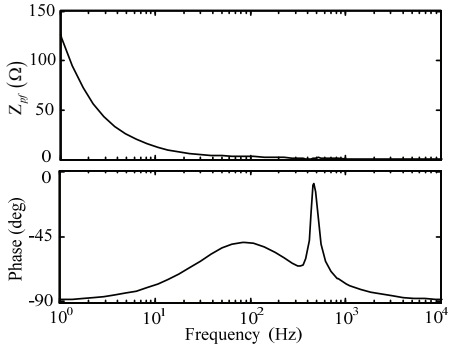

Fig. 2 Frequency response of the DCPF.

According to the DCPF parameters detailed in the Appendix, the frequency response of Z_{pf} is shown in Fig. 2. The DCPF, which acts like a high pass filter, provides a low impedance path to frequencies higher than 100 Hz and can substantially decrease the flat-top ripple of the magnet.

Power supply control strategy

3.1 Magnet resistance

When a high current flows through the magnet, the temperature increases, resulting in increasing the resistance and specific heat of the magnet. The resistance variation of the magnet is affected by three factors: the current, the resistivity and the specific heat. A resistance circuit model of the pulsed magnet with the concept of an iterative algorithm is utilized [11]:

$$\begin{cases} i_m^2(t)R_m(t)dt = c(t)M_a dT \\ R_m(t) = R_{m0} + \alpha_m \Delta T \\ c(t) = c(T) \end{cases} \tag{3}$$

where t is the time, $i_m(t)$ is the coil current of the magnet, $R_m(t)$ is the magnet resistance proportional to the temperature, α_m is a coefficient, the initial resistance of the magnet is R_{m0}, $c(t)$ is the specific heat as function of time, $c(T)$ is the specific heat function of the temperature, M_a is the mass of the magnet, ΔT is the increment of the temperature, the initial temperature T_0 is 77 K. Fig. 3 shows the curves of the magnet resistance R_m coinciding with the magnet temperature versus time during a pulse. $R_m(t)$ changes from 3.50 mΩ to 11.67 mΩ as the temperature drifts from 77 K to 155 K. All the magnet parameters are given in the Appendix.

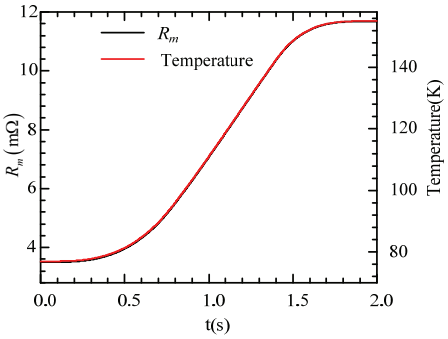

Fig. 3 Magnet resistance and temperature during a long pulse.

3.2 Control of PCR

The aim of the control scheme adopted in this paper is to maintain the HFQCM flat-top field constant and reduce the dc current ripple to an extremely small value. This is achieved by controlling the firing angle α during the pulse period.

Under continuous-current operating conditions, the PCR output voltage u_{dc} may be represented by

$$u_{dc} = \bar{u}_{dc} + \tilde{u}_{dc} \tag{4}$$

Where

$$\begin{cases} \bar{u}_{dc} = \dfrac{m}{2\pi}\displaystyle\int_{-\frac{\pi}{m}+\alpha}^{\frac{\pi}{m}+\alpha} \left(\sqrt{2}U_2 \cos\omega t\right) d(\omega t) \\ \tilde{u}_{dc} = \displaystyle\sum_{n=mk}^{\infty} C_n \cos(n\omega t - \theta_n) \end{cases} \tag{5}$$

$$\begin{cases} a_n = \dfrac{m}{\pi}\displaystyle\int_{-\frac{\pi}{m}+\alpha}^{\frac{\pi}{m}+\alpha} \left(\sqrt{2}U_2 \cos\omega t \bullet \sin n\omega t\right) d(\omega t) \\ b_n = \dfrac{m}{\pi}\displaystyle\int_{-\frac{\pi}{m}+\alpha}^{\frac{\pi}{m}+\alpha} \left(\sqrt{2}U_2 \cos\omega t \bullet \cos n\omega t\right) d(\omega t) \\ C_n = \sqrt{a_n^2 + b_n^2} \end{cases} \tag{6}$$

and $n=mk$, $m=6$, $k=1, 2, 3...$

It may be noted that as in the case of the PCR, for which the corresponding expressions are given in equations (4) ~ (6), the ripple voltage $\tilde{u}_{dc}$ is a function of α. In Fig. 4 are shown curves of the normalized ripple amplitude $d_n = C_n/\sqrt{2}U_2$ versus α with n as a parameter [12]. Considering both the minimization of $\tilde{u}_{dc}$ and the overlap angle limitation, it is strongly suggested to work within the recommended working area for the PCR in the converter mode. For this reason, one goal for the PCR control is to keep α as small as possible during the flat-top of the magnetic field. However, not only the control method, but also the secondary voltage U_2 on the transformer and the magnet parameters may affect the control of α.

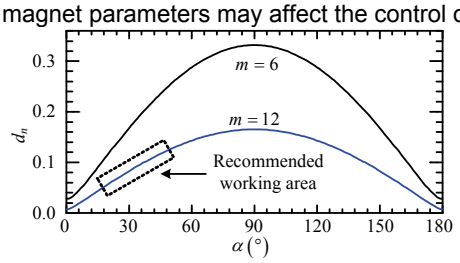

Fig. 4 d_n versus α with n as a parameter.

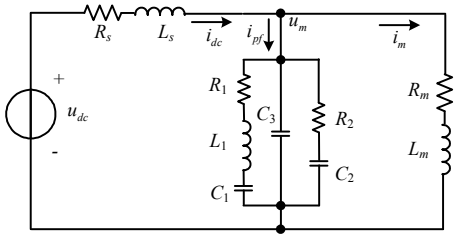

Fig. 5 The equivalent power circuit.

The equivalent power circuit of the whole system is shown in Fig. 5, where R_s and L_s are the resistance and the inductance of the smoothing reactor, R_m and L_m represent the magnet load, and R_1, L_1, C_1, R_2, C_2, and C_3 represent the DCPF.

Based on Kirchhoff's current law, the functions of the power supply are given by

$$\begin{cases} u_{dc} - u_m = i_{dc} Z_s \\ u_m = i_{pf} Z_{pf} \\ u_m = i_m Z_m \\ i_{dc} = i_m + i_{pf} \end{cases} \tag{7}$$

where

$$\begin{cases} Z_s = R_s + sL_s \\ Z_m = R_m + sL_m \end{cases} \tag{8}$$

Substituting (8) in (7), the transfer function of the control object can be expressed as

$$G_{obj} = \frac{i_m}{u_{dc}} = \frac{1}{Z_s} \bullet \frac{1}{1 + (Z_m/Z_s) + (Z_m/Z_{pf})} \tag{9}$$

Under several assumptions, the PCR can be represented as a dead-time element [13]:

$$G_{PCR} = K_{rt} e^{-\alpha_d s} \tag{10}$$

where

$$\begin{cases} K_{rt} = 0.9U_2 \\ \alpha_d = 1/(12\omega_s) \end{cases} \tag{11}$$

Conventionally, K_{rt} is the steady-state gain of the PCR and the dead-time delay can be considered as one-twelfth of the ac source angle.

The PCR controller is a feedback controller, which provides pole-zero cancellation for the R_m-L_m plant. This is a complex-coefficient PI controller, with cross-coupling decoupling and with the feed-forward control of the reference of the firing angle α_{ref}.

$$G_{PI} = \frac{K_p(\tau_i s + 1)}{\tau_i s} \tag{12}$$

Assuming ω_s and R_m constant, The PI parameters K_p and τ_i are selected as $\tau_i = L_m / R_m$, with K_p small, such that the controller has relatively slow response, which does not interfere with the feed-forward controller. But the current control loop must be designed faster than the feed-forward controller to get a good performance. A system block diagram of the proposed magnet power supply system, including the controller (12), the PCR model (10) and the target model (9), is shown in Fig. 6.

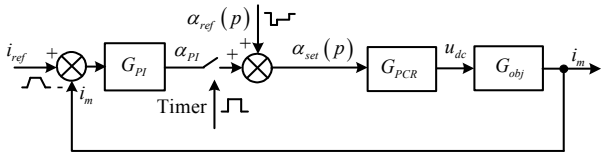

Fig. 6 The PCR control loop.

The control system contains two parts: one is the firing angle open loop, the other is the current closed loop. $\alpha_{ref}(p)$ is the reference of the firing angle at the pulse number p. $\alpha_{set}(p)$ is the output firing angle of the PCR control system. α_{PI}, the output of the closed loop, is limited ±20 °. As a result of the control strategy, the coil current may climb to about 40 kA during a pulse. The precise measurement of such high level is a real challenge. The device selected for the PCR control system might use the zero-flux-principle DCCT [14][15].

The Bode plot of the PCR closed loop is drawn in Fig. 7. Depending on the value of K_p, the attenuation at the frequency 1 kHz may be better or worse. When $K_p = 0.05$, it is demonstrated that there might be a magnitude amplification at the frequency 200 Hz. Nevertheless, it is confirmed in the simulations that oscillations always exist when $K_p \geq 0.1$. It is suggested that K_p is selected to a small value such that the oscillation could be prevented. But the effect of changing K_p must be also thought of how much the closed loop working on the whole system.

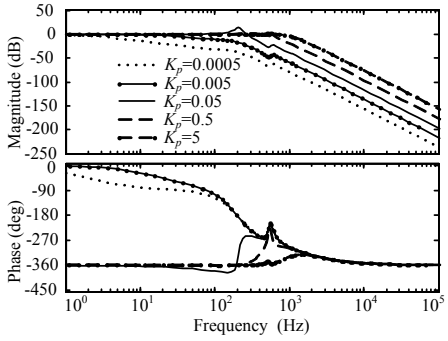

Fig. 7 Bode plot of the PCR closed loop.

Considering the stability and the minimization of the tracking error by selecting K_p, a repetitive control method is proposed. Both $\alpha_{ref}(p)$ and $\alpha_{set}(p)$ are memorized at the end of each pulse. A timer is set up to make sure that the closed loop functions only at the flat-top duration.

$$\alpha_{set}(p) = \alpha_{ref}(p) + \alpha_{PI} \tag{13}$$

where p = 1, 2, 3...

When it is the first pulse, $\alpha_{set}(1)$ is a completely open loop. When it is at the pulse number $p(p \geq 2)$, let

(14) $$\alpha_{ref}(p) = \alpha_{set}(p-1)$$

This means that $\alpha_{set}(p)$ contains the tracking error information from the last pulse. After several pulses, for example, $p \geq 6$, α_{PI} decreases to almost zero. The PCR is then controlled approximately, in an open-loop fashion. Moreover, it responds faster to reference change and is not limited by the ramp rate of the current reference. Because of the open-loop nature, it does not have the adverse effects of delay, overshoots, or oscillations existing in a feedback system.

Results

A number of measurements at primary power conditions was made during the current stability simulations, and the results are as follows.

Fig. 8 gives the coil current waveforms which always coincide with the magnetic field curves under the feed-forward control and the proposed repetitive control at pulse number 1, 2 and 6. With the feed-forward control only, the flat-top of the magnetic field cannot be maintained because of the nonlinear magnet resistance. As expected, the magnetic field waveform can be improved by the proposed control. The coil current amounts to 39.98 kA, the magnetic field reaches 45.45 T closely, and the flat-top time extends to almost 600 ms. By including the DCPF, the ripple of the coil current is greatly reduced. This can be seen more clearly from the steady state waveform in the inset in Fig. 8. Furthermore, the peak-to-peak ripple is highly attenuated at the 2 A level, and the ripple factor achieves about 25 ppm.

Fig. 9 and Fig. 10 show magnet voltages and the referential firing angles related at pulse number 1, 2 and 6 respectively. During the 6th pulse, as a result of the rise of magnet resistance, the magnet voltages also rise during the flat-top period, which keeps the magnetic field nearly constant. Fig. 11 shows the DCPF current at pulse number 6. Fig. 12 shows how the FPG shaft speed changes at the pulse number 6. The PCR has to be fully operational across the entire pulse operation frequency-range of the FPG, i.e. 713 rpm to 665 rpm.

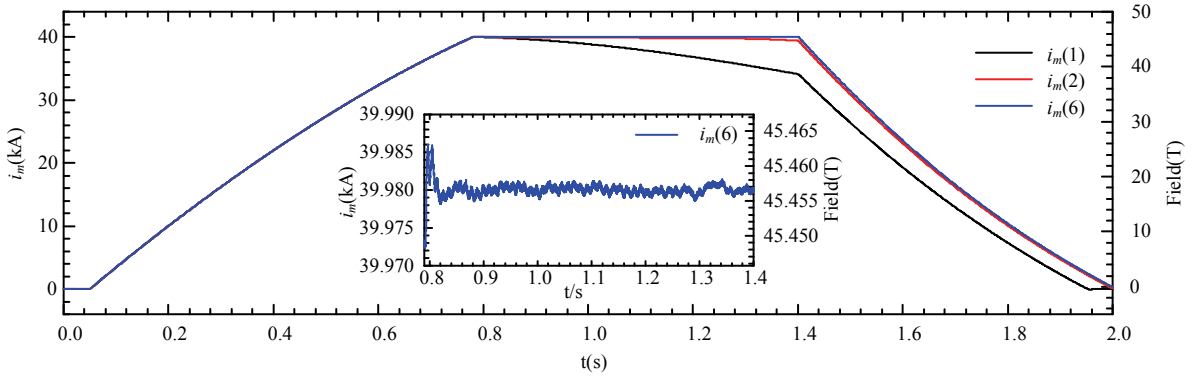

Fig. 8 Coil current waveforms and field curves in three modes of operation.

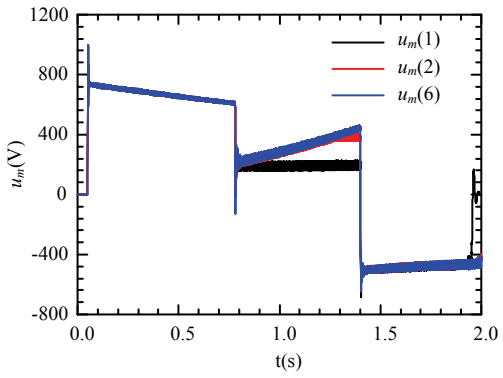

Fig. 9 Magnet voltages at pulse number 1, 2 and 6.

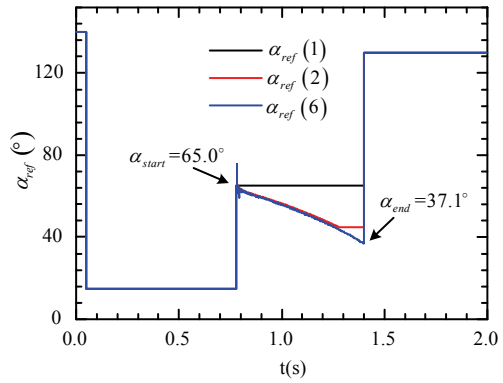

Fig. 10 Referential firing angles at pulse number 1, 2 and 6.

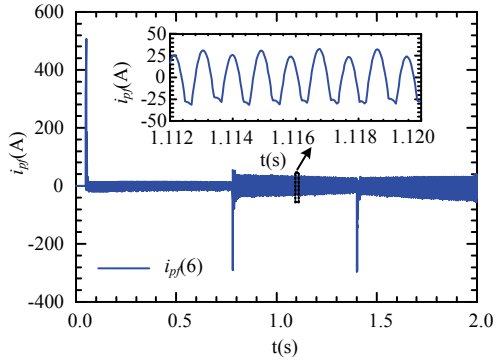

Fig. 11 DCPF current at pulse number 6 as a function of time.

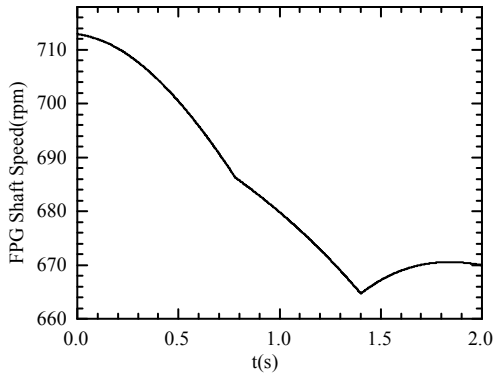

Fig. 12 FPG shaft speed at pulse number 6 as a function of time.

Conclusions

The repetitive control method for the HFQCM power supply provides a means to reduce the ripple of the coil current and increase the operational flexibility. The operating principle, simplified control design and feasibility simulations have been presented. Steady-state simulation studies adopting the proposed control strategy show that the coil current will be kept constant during the flat-top time by controlling the firing angle *α*. It is conclusively demonstrated that the elimination of the current ripple can be accomplished by installing a DCPF at the output of the PCR. Furthermore, a dc active power filter, cooperating with the DCPF at the WHMFC, is already included in the schedule. Related research results will be published in the near future. The tuned filters for the 11th and 13th harmonics installed at the output of the FPG will be discussed later.

Appendix

1) FPG parameters:

Type: Salient pole; synchronous; 3 phase alternator.

Number of poles: 16.

Initial frequency: 95 Hz.

Rotating speed ω_s: 713 rpm ~ 495 rpm.

Rate of power: 100 MVA.

Energy storage: 185 MJ.

WR^2 (set): 1.6×10^6 lbft^2.

2) PCR parameters:

6.9 kV/0.66 kV transformers.

R_s = 1.0 mΩ, L_s = 2.2 mH.

K_p = 0.08.

Sampling time: 1 ms.

3) DCPF parameters:

R_1 = 1.0 Ω, L_1 = 2.2 mH, C_1 = 60 μF, R_2 = 4.0 Ω, C_2 = 1000 μF, C_3 = 200 μF.

4) Magnet parameters:

$L_m = 10.56$ mH , $\alpha_m = 0.173$, $R_{m0} = 3.5$ mΩ , $T_0 = 77.0$K , $M_a = 500.0$ kg .

REFERENCES

[1] H. Jin, Y. Wang and G. Joos, A Hybrid Structure Using Phase-Controlled Rectifiers and High-Frequency Converters for Magnet-Load Power Supplies, *IEEE Trans. Ind. Electron.*, 43 (1996), No. 1, 126-131.

[2] Y. Wang, G. Joos and H. Jin, DC-Side Shunt-Active Power Filter for Phase-Controlled Magnet-Load Power Supplies, *IEEE Trans. Power Electron.*, 12 (1997), No. 5, 765-771.

[3] H. Jin and S. B. Dewan, A Combined Feed-Forward and Feedback Control Scheme for Low-Ripple Fast-Response Switch Mode Magnet Power Supplies, *IEEE Trans. Magn.*, 30 (1994), No. 4, 1801-1804.

[4] L. Li, H. F. Ding, T. Peng, et. al., The Pulsed High Magnetic Field Facility at HUST, Wuhan, China and Associated Magnets, *IEEE Trans. Appl. Supercond.*, 18(2008), No. 2, 596–599.

[5] J. B. Schillig, H. J. Boenig, M. Gordon, et. al., Operating Experience of the United States National High Magnetic Field Laboratory 60T Long Pulse Magnet, *IEEE Trans. Appl. Supercond.*,10 (2000), No. 1, 526-529.

[6] J. B. Schillig, H. J. Boenig, J. D. Rogers, et. al., Design of a 400MW Power Supply for a 60T Pulsed Magnet, *IEEE Trans. Magn.*, 30 (1994), No. 4, 1770-1773.

[7] L. J. Campbell, H. J. Boenig, D. G. Rickel, et. al., Status of the NHMFL 60 Tesla Quasi-Continuous Magnet, *IEEE Trans. Magn.*, 32 (1996), No. 4, 2454-2457.

[8] G. Zhuang, Y. H. Ding, M. Zhang, et. al., Reconstruction of the TEXT-U Tokamak in China, *Plasma Science and Technology*, 11 (2009), No. 4, 439-442.

[9] W. F. Praeg, A High-Current Low-Pass Filter for Magnet Power Supplies, *IEEE Trans. Ind. Elec. and Control Instrum.*, IECI-17 (1970), No. 1, 16-22.

[10] K. Li, J. J. Liu, G. C. Xiao, et. al., Novel Load Ripple Voltage-Controlled Parallel DC Active Power Filters for High Performance Magnet Power Supplies, *IEEE Trans. Nucl. Sci.*, 53 (2006), No. 3, 1530-1539.

[11] F. Herlach and N. Miura, High Magnetic Fields Science and Technology, Singapore: World Scientific Publishing, 2003.

[12] S. B. Dewan and A. Straughen, Power Semiconductor Circuits, New York: John Wiley & Sons, 1975.

[13] R. Liang and S. B. Dewan, Modeling and Control of Magnet Power Supply System with Switch-Mode Ripple Regulator, *IEEE Trans. Ind. Appl.*, 31 (1995), No. 2, 264-272.

[14] H. J. Boenig, F. Bogdan, G. C. Moms, et. al., Design and Preliminary Test Results of the 40 MW Power Supply at the National High Magnetic Field Laboratory, *IEEE Trans. Magn.*, 30 (1994), No. 4, 1774-1777.

[15] H. J. Boenig, J. A. Ferner, F. Bogdan, et. al., Design and Operation of a 40-MW, Highly Stabilized Power Supply, *IEEE Trans. Ind. Appl.*, 32 (1996), No. 5, 1146-1157.

***Authors**: dr. Weiwei Liu, Huazhong University of Science and Technology Luoyu str. 1037, Wuhan, China, E-mail: loudi_liuvv@foxmail.com. prof. Hongfa Ding, Huazhong University of Science and Technology Luoyu str. 1037, Wuhan, China, E-mail: dinghongfa@sina.com.cn. prof. Xianzhong Duan, Huazhong University of Science and Technology Luoyu str. 1037, Wuhan, China, E-mail: xzduan@hust.edu.cn. prof. Liang Li, Huazhong University of Science and Technology Luoyu str. 1037, Wuhan, China, E-mail: liangli44@mail.hust.edu.cn. prof. Fritz Herlach, E-mail: fritz.herlach@fys.kuleuven.be.*

The correspondence address is:

e-mail: loudi_liuvv@foxmail.com